Theoretical calculation of ozone vibrational infrared intensities

Steven M. AdlerGolden, Stephen R. Langhoff, Charles W. Bauschlicher, and Grady D. Carney

Additional information on J. Chem. Phys.
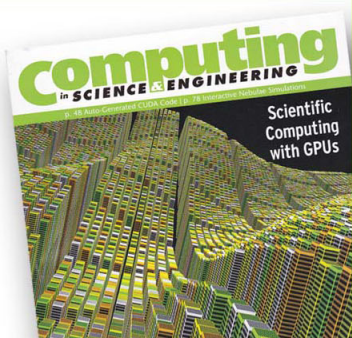
Theoretical calculation of ozone vibrational infrared intensities

Steven M. Adler-Golden

Spectral Sciences, Inc., Burlington, Massachusetts 01803

Stephen R. Langhoff and Charles W. Bauschlicher, Jr.

NASA/Ames Research Center, Moffett Field, California 94035

Grady D. Carney

Department of Chemistry, Allegheny College, Meadville, Pennsylvania 16335

An *ab initio* dipole moment function for ozone has been computed using the CASSCF (complete active space self-consistent field) method, and forms the basis for a calculation of ozone infrared band intensities. Vibrational wave functions were generated using the variational method with potential energy surfaces derived from experimental force constants. Computed values of the permanent dipole moment, dipole moment derivatives, and infrared band strengths are all found to be in remarkably good agreement with experiment. Intensities are predicted for hot bands for which experimental values are unavailable, and implications for atmospheric ozone spectroscopy are discussed. As the dipole moment matrix element signs are now established for nearly all of the observed bands, further refinement of the dipole moment function is possible.

I. INTRODUCTION

As the ozone molecule is one of the most important species in the earth's atmosphere, its spectral properties have been the subject of intensive study. Of particular interest is its infrared spectrum, which is prominent in long path absorption, and which has also been seen in emission in the upper atmosphere. Recently, new attention has focused on the properties of ozone's excited vibrational levels, motivated in large measure by the observation of atmospheric emission in the 10 μ (ν_3) band resulting from the $O + O_2 \rightarrow O_3$ recombination process.[1] Further studies have been conducted by Rawlins *et al.*[2,3] at the Air Force Geophysics Laboratory's COCHISE facility, which provides a low pressure, cryogenic environment for the observation of infrared chemiluminescence. These experiments have identified ozone 10 μ chemiluminescence from vibrational levels containing as many as five stretching quanta. This hot band emission, which is red shifted from the ν_3 fundamental, may provide a significant source of infrared background radiation in the upper atmosphere. Some ozone hot bands also appear in atmospheric absorption spectra, and need to be taken into account in applications such as the detection of trace gases.

As the bulk of our knowledge of ozone infrared properties is derived from ambient temperature absorption experiments, which observe mainly transitions from the ground vibrational state, considerably less is known about hot band properties. To better understand ozone infrared spectroscopy, and, in particular, to permit vibrational level populations to be derived from hot band spectra, we have undertaken the theoretical calculation of ozone pure vibrational intensities. The intensities may be expressed either in terms of the Einstein A coefficient,

$$A /s^{-1} = 2.026 \times 10^{-6} (\bar{\nu}/cm^{-1})^3 (R /ea_0)^2 \tag{1}$$

or in terms of the band strength S,

$$S /atm^{-1} cm^{-2} \text{ at } 298 \text{ K} = 66.15 (\bar{\nu}/cm^{-1})(R /ea_0)^2, \tag{2}$$

where $\bar{\nu}$ is the wave number of the band origin and R is the dipole moment matrix element in atomic units ($1ea_0 = 2.541\ 77$ D). The results presented in this paper are based on a new *ab initio* dipole moment function which was generated using the CASSCF (complete active space self-consistent field) method, and which constitutes a great improvement over previous calculations. For the potential energy function a polynomial expansion derived from experimental force constants was used. The vibrational analysis was carried out using the variational method to generate accurate vibrational wave functions. With this approach we have obtained remarkably good agreement with fundamental, overtone, and combination band intensities observed in infrared absorption from the ground vibrational state. We feel that the calculated hot band intensities are comparably reliable, and will be valuable for the modeling of atmospheric and laboratory spectra. Moreover, since ambiguities in the signs of the dipole moment matrix elements have now been resolved, the dipole moment can be further refined using the experimental band strengths.

II. *AB INITIO* DIPOLE MOMENT AND POTENTIAL ENERGY SURFACES FOR OZONE

The dipole moment and potential energy surfaces were calculated using two different Cartesian basis sets. For generating the global surfaces a standard double-zeta plus polarization (DZP) basis was used which consisted of the $(9s5p)$ set of Huzinaga[4] contracted to $[4s2p]$ according to Dunning,[5] augmented with a d function with an orbital exponent of 0.85. In addition, to study the sensitivity of the dipole moment and its first derivatives to basis set quality, calculations were performed at points near the equilibrium geometry using a $(11s6p2d)$ $[6s3p2d]$ triple-zeta plus double polarization (TZ2P) basis. The $6s3p$ basis consisted of the $[611111/411]$ contraction of van Duijneveldt,[6] and was augmented with two d functions ($\alpha = 0.85$ and 0.20).

In C_{2v} symmetry the ground state of ozone can be written as

0021-9606/85/130255-10$02.10

$$1a_1^2 \cdots 6a_1^2 \; 1b_1^2 \; 1b_2^2 \cdots 4b_2^2 \; 1a_2^2 \quad (^1A_1). \tag{3}$$

It is well known that the Hartree–Fock (HF) level provides a rather poor description of the biradical character of the $^1A_1$ ground state. The first qualitatively correct description of the bonding is given by the two-configuration generalized valence bond (GVB) wave function, which can be written in C_{2v} symmetry as[7]

$$1a_1^2 \cdots 6a_1^2 \; 1b_1^2 \; 1b_2^2 \cdots 4b_2^2 \; [c_1(1a_2^2) - c_2(2b_1^2)]. \tag{4}$$

The description of the wave function can be further improved with more elaborate GVB wave functions constructed with correlating configurations involving both the σ and π electrons. We have also considered all single- and double-excitation configuration-interaction [CI(SD)] wave functions from both the HF and GVB (two-configuration) references with a variety of molecular orbital bases. Finally, we have considered complete active space self-consistent field (CASSCF)[8,9] wave functions in which the 12 $1s$ and $2s$ electrons were inactive (doubly occupied) and the 12 $O(2p)$ electrons were active.

In Table I we have summarized the effects of electron correlation on the dipole moment of ozone near the equilibrium geometry using both the DZP and TZ2P basis sets. At nearly all levels of correlation the TZ2P basis gives a slightly smaller magnitude for the dipole moment, owing to the somewhat more diffuse nature of the wave functions when the diffuse d function is included. Once the basis sets reach DZP quality, the magnitude of the dipole moment is significantly overestimated at the HF level, but significantly underestimated at the GVB level, mainly through changes in the doubly occupied orbitals. As more configurations are added to the GVB, the dipole moment increases in magnitude, and the occupied orbitals more closely resemble those

obtained from HF. These same trends can be seen in the CI(SD) results as well. All singles and doubles from the HF configuration, although better than HF, still results in a dipole moment that is larger in magnitude than experiment. Similarly, the two-reference CI(SD) dipole moment (using GVB orbitals), although significantly better than GVB, is still too small. The two-reference CI(SD) result is further improved upon a natural orbital iteration. Also, from Table I one can see that the dipole moment is significantly better when a mixed orbital set is used (HF occupied orbitals combined with GVB $2b_1$ and virtual orbitals). These results suggest the need for a balanced treatment of both the correlation and orbital optimization, such as in the CASSCF approach. The CASSCF wave functions produce dipole moments in quantitative accord with experiment, differing only by about 0.02 D between the two bases. This good agreement suggests that the CASSCF wave function provides a balanced description of the charge distribution in ozone, as has been the case in previous POLCI treatments.[10]

In Table II we compare the dipole moment first derivatives computed with both the DZP and TZ2P basis sets at the CASSCF level with those obtained from experimental infrared intensity data.[11] (The dipole moment vector components are given as μ_{xVAB} and μ_{yVAB}, where the x_{VAB} axis is defined as the valence angle bisector, and the y_{VAB} axis is perpendicular to x_{VAB} and directed towards the r_1 side of the molecule; this is consistent with Fig. 1 of Ref. 12.) The derivatives are found to be in far better agreement with experiment than previous HF and selected CI(SD) results.[13] The derivatives using the TZ2P basis are in particularly good agreement with experiment, suggesting that a diffuse d function is required for very quantitative results.

The goal of the present study was to construct a global dipole moment surface for ozone that extended to large enough displacements to allow the determination of overtone, combination and hot band intensities. The CASSCF method was selected not only because of its quantitative description of the dipole moment and its first derivatives, but

TABLE I. Basis set and correlation effects on the dipole moment of ozone.

Description of method	Dipole moment/D	
	DZP[a]	TZ2P[a]
HF	− 0.830	− 0.766
GVB	− 0.127	− 0.141
GVB + $\pi^2 \to \pi^{*2}(1b_1^2 \to 2b_1^2)$		− 0.203
GVB + $\sigma^2 \to \sigma^{*2}$	− 0.238[b]	
GVB + $\pi^2 \to \pi^{*2} + \sigma^2 \to \sigma^{*2}$	− 0.317[b]	
CI (SD) from HF reference	− 0.709	− 0.668
CI (SD) from two-references (GVB) using GVB orbitals	− 0.356	− 0.339
CI (SD) from two-references (GVB) using natural orbitals from previous CI		− 0.402
CI (SD) from two-reference (GVB) using HF occupied orbitals and GVB virtual orbitals		− 0.534
CASSCF with $1s$, $2s$ orbitals inactive, $2p$ orbitals active	− 0.557	− 0.536
Experimental	− 0.532 ± 0.002[c]	

[a] Calculated at $r = 1.278$ Å, $\theta = 116.8°$; see the text for description of the basis sets. The positive direction is taken as the valence angle bisector vector.

[b] Carried out in C_s symmetry to allow the orbitals to localize, thus minimizing the number of configurations included. Note that the overall wave function has C_{2v} symmetry even though the individual orbitals do not.

[c] Absolute value measured in Ref. 15.

TABLE II. Ozone dipole moment first derivatives using CASSCF wave functions. Units are D, Å, and rad.

Derivative[a]	DZP[b]	TZ2P[b]	Expt.[c]
$\dfrac{\partial \mu_{xVAB}}{\partial r}$	0.87	0.78	0.76
$\dfrac{\partial \mu_{xVAB}}{\partial \theta}$	0.95	0.83	0.74
$\dfrac{\partial \mu_{yVAB}}{\partial r}$	− 2.41	− 2.45	− 2.60

[a] The derivatives are the coefficients in the Taylor expansions

$$\mu_{xVAB} = \mu_0 + \frac{\partial \mu_{xVAB}}{\partial r}(\Delta r_1 + \Delta r_2) + \frac{\partial \mu_{xVAB}}{\partial \theta}\Delta \theta$$

and

$$\mu_{yVAB} = \frac{\partial \mu_{yVAB}}{\partial r}(\Delta r_1 - \Delta r_2).$$

[b] Evaluated at $r = 1.278$ Å, $\theta = 116.8°$.

[c] From Ref. 11, obtained by fitting the dipole moment to infrared intensity data, and evaluated at the experimental equilibrium geometry, $r = 1.272$ Å, $\theta = 116.8°$.

also because the method uses a fixed configuration list, and is therefore capable of high precision, especially when quadratic convergence is employed. All calculations were carried out in C_s symmetry to ensure that no discontinuities arose upon asymmetric bond stretches. In C_s symmetry using the DZP basis the CASSCF included 1292 CSF's, which includes all possible arrangements of the 12 valence O(2p) electrons in nine active 2p orbitals. The CASSCF energy and dipole moment were evaluated at over 200 geometries which thoroughly covered the range of vibrational energies from 0 to 1 eV for bond lengths of up to 1.754 Å. As will be shown in Sec. V, the good agreement between the experimental and calculated band strengths suggests that this *ab initio* dipole moment function is reasonably accurate over the range of geometries probed by the vibrational states considered.

Near the equilibrium geometry the shape of the CASSCF potential energy surface is quite accurate. We have obtained values for the equilibrium bond length and internal angle and internal coordinate force constants by performing least squares polynomial fits to the grid of potential energy values. The calculated equilibrium bond length r_e is 1.2956 Å, which is only slightly longer than the experimental value[14,15] of 1.2717 Å, while the equilibrium angle θ_e is 116.5°, essentially identical to the experimental value of 116.8°. Another measure of the accuracy of the potential surface is provided by the force constants, which are the coefficients K_{ijk} in the Dunham expansion

$$V = r_e^2 \sum_{ijk} K_{ijk}(x_1^i + x_2^i)(x_1 x_2)^j x_3^k / (1 + \delta_{0i}),\qquad(5)$$

where $x_1 = \Delta r_1/r_e$, $x_2 = \Delta r_2/r_e$, $x_3 = \Delta \theta$ (Δr_i and $\Delta \theta$ denote displacements relative to equilibrium); $\delta_{0i} = 1$ when $i = 0$ and $\delta_{0i} = 0$ otherwise. To facilitate comparison with experimental force constants we took r_e in the above expression as 1.2717 Å, while the Δr_i were taken relative to the calculated equilibrium distance of 1.2956 Å. This effectively shifts the CASSCF surface to match the experimental equilibrium distance. We derived force constants from two separate fits to test for stability. The quadratic and cubic force constants were found to be stable, and appear in Table III. They agree very well with experimental values derived from rotation-vibration spectral analysis.[16,17]

TABLE III. Quadratic and cubic force constants of the DZP CASSCF potential energy surface for ozone (10^{-12} erg/Å^2).

i	j	k	Fit 1[a]	Fit 2[b]	Experimental[c]
0	1	0	17.1	17.1	16.02
0	1	1	− 15.4	− 11.9	− 13.0
0	0	2	6.30	6.29	6.5
0	0	3	− 3.68	− 3.60	− 3.9
1	1	0	− 9.13	− 11.2	− 16.8
1	0	1	3.61	3.64	4.02
1	0	2	− 15.1	− 14.4	− 15.4
2	0	0	27.4	27.9	30.815
2	0	1	− 6.37	− 8.74	− 15.8
3	0	0	− 116.9	− 118.4	− 116.4

[a] Sixth degree Dunham polynomial, 50 terms, $\sigma = 0.0060 \times 10^{-12}$ erg.
[b] Fifth degree Dunham polynomial, 34 terms, $\sigma = 0.0075 \times 10^{-12}$ erg.
[c] From Ref. 16.

As a further test of the CASSCF potential energy surface, we calculated the frequencies of the lowest few vibrational levels using the variational procedure described in Sec. IV; the results are presented in Table IV. Agreement with the experimental values is within 2% to 11%, which is consistent with the small error in the quadratic force constants.

Although the CASSCF calculation is size consistent, the computed binding energy is only about 0.5 eV, compared to the experimental value of 1.1 eV,[18] owing to the fact that the calculation recovers only a portion of the extra molecular correlation energy. The surface is thus not globally accurate, and would not be appropriate for studying the dissociative pathways of ozone. The dipole moment surface should be less sensitive to the missing correlation energy and should therefore be more globally accurate. In fact, we feel that extending the dipole moment surface to the TZ2P CASSCF level would be more accurate and precise than extending the DZP CASSCF with a CI(SD) from the important references in the CASSCF. It would be difficult to extend to the CI(SD) level in a precise way because there are many important references that change with geometry in the CASSCF wave functions.

Given the limitations of the CASSCF potential energy surface, especially at large vibrational amplitudes, we next consider alternative potential surfaces which are more suitable for the calculation of ozone infrared intensities.

III. IMPROVED OZONE POTENTIAL ENERGY SURFACES

A. Available potential energy surfaces

A number of potential energy surfaces for ozone derived from observed spectra have appeared in the literature. One class of surfaces is in a functional form due to Sorbie and Murrell[19,20] which insures proper dissociation to products. The most recent of these surfaces, that of Carter *et al.*,[21] reproduces the observed band frequencies reasonably well, but contains cubic and quartic force constants which differ considerably from the experimental ones. This is of particular concern in the case of the cubic force constants, whose experimental values should be very reliable as they derive from rotational constants measured from high resolution spectra.

An alternative approach which incorporates the experi-

TABLE IV. Vibrational energy levels of the DZP CASSCF potential energy surface for ozone (cm^{-1}).

v_1	v_2	v_3	Calculated[a]	Experimental (Ref. 16)
0	1	0	684	701
0	0	1	928	1042
1	0	0	1050	1103
0	2	0	1364	1399
0	1	1	1589	1727
1	1	0	1721	1795
1	0	1	1911	2111

[a] Sixth degree Dunham polynomial, 147 basis functions per vibrational symmetry.

mental force constants is to use a potential function consisting of a polynomial in suitable expansion variables such as the Simons–Parr–Finlan[22,23] (SPF) variables $\Delta r_1/r$, $\Delta r_2/r$, and $\Delta\theta$. The force constants C_{ijk} associated with this new set of variables are defined in a way such that when the Taylor expansion (5) in the Dunham variables x_i is taken, the coefficients K_{ijk} are exactly the experimental force constants. Carney *et al.*[23] have applied this method to water and ozone, obtaining improved band centers by using SPF variables instead of Dunham variables. The optimum ozone results were, however, obtained by using a potential energy function which is a linear combination of the two expansions.

While an SPF or other expansion variable potential energy function cannot exhibit proper long range behavior at all geometries, it can do a reasonably good job at modest bending angles.[22] Moreover, its polynomial form is highly efficient for our variational program, as it avoids the need for a three-dimensional integration to evaluate potential energy matrix elements. Thus, for both the sake of accuracy and efficiency, we used an expansion variable polynomial as our potential energy function in the following calculations. However, to study higher-lying vibrational states a more realistic potential energy surface will be required.

B. Choice of expansion variables

Calculations were performed using three different expansion variable potential energy surfaces. The force constants were taken as the experimental values from Barbe *et al.*[16] The first surface was the Dunham expansion, which as discussed in Sec. IV was used mainly as a test of our variational algorithm, since it gives rather poor agreement with experimental energy levels. Next, we used the SPF variables and obtained improved results similar to those given previously.[23] Finally, hoping to further improve upon the calculated energy levels, we tried the set of expansion variables given by

$$y_1 = \frac{1 - \exp(-\alpha\Delta r_1)}{\alpha r_e}, \tag{6}$$

$$y_2 = \frac{1 - \exp(-\alpha\Delta r_2)}{\alpha r_e}, \tag{7}$$

$$y_3 = \Delta\theta, \tag{8}$$

which are the expansion variables appropriate for treating the bond stretches as Morse-like oscillators.[24,25] We shall refer to the potential surface based on the variables (6)–(8) as the MPMO potential, since it is a multidimensional generalization of the potential function which Refs. 24 and 25 call the perturbed Morse oscillator (PMO). The algebra for generating the MPMO force constants from Dunham force constants is given in Appendix A. We performed calculations with two different α values, 2.5 and 2.7192 Å^{-1}. The former value is appropriate for the oxygen molecule, while the latter was chosen to give a zero quartic expansion coefficient C_{400} and a nearly zero cubic coefficient C_{300} (see Appendix A). The calculated vibrational energy levels differed by at most 2 cm^{-1} for the two different values of α.

A comparison of experimental and calculated vibrational energy levels using the MPMO potential function ap-

TABLE V. Vibrational energy levels of ozone (cm^{-1}) relative to the ground state (0 0 0).

State	v_1	v_2	v_3	Exptl.[a]	MPMO[b]	Carter[c] *et al.*
2A	0	1	0	700.9	700.5(0.1)	701
1B	0	0	1	1042.1	1042.4(0.0)	1043
3A	1	0	0	1103.1	1101.1(0.1)	1103
4A	0	2	0	1399.3	1397.4(0.1)	...
2B	0	1	1	1726.5	1724.7(0.0)	1730
5A	1	1	0	1795.3	1792.2(0.2)	1790
6A	0	0	2	2058.0	2059.8(0.6)	2061
7A	0	3	0	...	2088.5(1.1)	...
3B	1	0	1	2110.8	2108.6(0.2)	2112
8A	2	0	0	2201.3	2196.6(0.3)	2201
4B	0	2	1	2409.5	2401.6(0.2)	2409
9A	1	2	0	...	2482.3(1.5)	...
10A	0	1	2	2725.6	2724.9(1.7)	2736
5B	1	1	1	2785.2	2781.5(0.5)	2786
12A	2	1	0	...	2874.5(1.4)	...
6B	0	0	3	3046.0	3050.9(1.1)	3054
7B	0	3	1	...	3071.1(1.4)	...
8B	2	0	1	3185.7	3183.0(0.6)	3207
15A	3	0	0	...	3282.8(1.5)	...

[a] Band origins from Ref. 16, except for the (0 2 0) state from Ref. 26.
[b] $\alpha = 2.7192$ Å^{-1}, 224 basis functions per vibrational symmetry. Number in parentheses is the change in energy when using 147 functions per vibrational symmetry. The zero point energy is 1454.9 cm^{-1}.
[c] Reference 21.

pears in Table V. The good agreement is comparable to that obtained with either the Carter *et al.* function[21] or the optimal Dunham-SPF function of Carney *et al.*,[23] and superior to that obtained with the pure SPF function. We have included several additional levels not reported in Refs. 21 or 23 which were well converged in our calculation.

At this point it is worthwhile to briefly discuss the variational vibrational analysis method used to generate the energy levels in Tables IV and V and the infrared intensities to be presented in Sec. V.

IV. VIBRATIONAL ANALYSIS METHOD

An overview of our procedure for generating vibrational energies and intensities is provided by the Fig. 1 flow chart. Force constants appropriate to the chosen set of expansion variables (Dunham, SPF, or MPMO) were generated from either experimental Dunham force constants or by least squares fitting the grid of *ab initio* points. Next, the force constants were input into our variational vibrational state program, which is based on the Carney–Cropek algorithm.[27] This algorithm solves the exact pure vibrational Hamiltonian in internal coordinates, generating energy levels and wave functions, and is described in detail elsewhere.[28] The basis functions are products of one-dimensional radial and angular wave functions. Although ideally suited for molecules such as water which have predominantly local-mode vibrational motion, this variational program also works quite well for ozone. With the Dunham expansion potential surface, ten quadrature points per vibrational coordinate, and a total of 448 basis functions (224 per vibrational symmetry) we achieved 0.3 cm^{-1} or better energy level agreement with a converged 1140-function calculation which used the Watson Hamiltonian in "t" coordinates.[23]
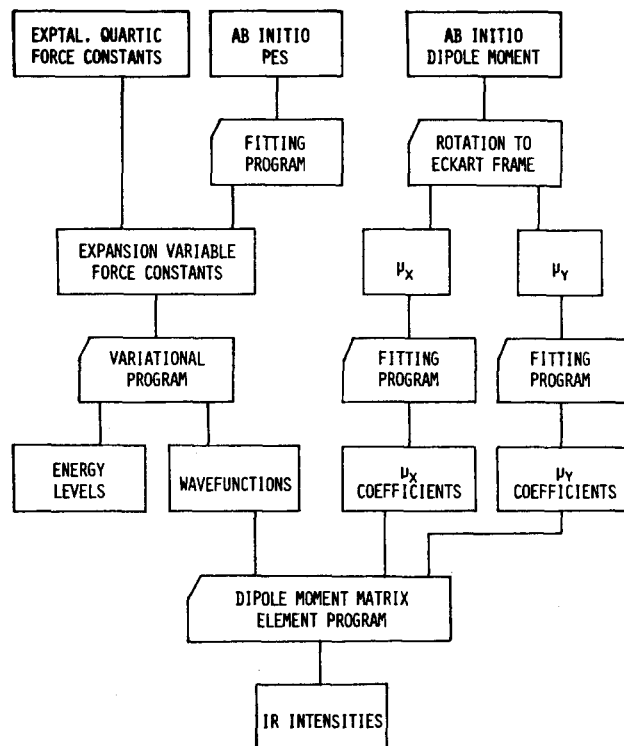
FIG. 1. Vibrational analysis flow chart.

TABLE VI. Coefficients of the dipole moment expansion in MPMO variables, $\alpha = 2.7192$ Å^{-1}; units are ea_0, Å, and rad. μ_x has the same functional form as the potential V in Appendix A. For μ_y the plus sign is changed to a minus sign.

i	j	k	$C_{ijk}(\mu_x)$	$C_{ijk}(\mu_y)$
0	0	0	− 0.129 280	
0	1	0	1.618 824	
0	2	0	73.329 074	
0	3	0	2038.330 737	
0	0	1	0.222 561	
0	1	1	− 1.694 511	
0	2	1	− 60.239 628	
0	0	2	0.051 054	
0	1	2	− 6.189 115	
0	2	2	60.192 979	
0	0	3	− 0.011 992	
0	1	3	5.451 635	
0	0	4	0.073 791	
0	1	4	9.835 044	
0	0	5	− 0.793 267	
0	0	6	0.731 255	
1	0	0	0.269 474	− 0.764 747
1	1	0	1.153 732	7.355 033
1	2	0	− 38.709 046	113.705 808
1	0	1	− 0.332 911	− 0.174 804
1	1	1	− 0.143 461	21.900 499
1	2	1	588.775 938	625.090 694
1	0	2	− 0.206 479	0.588 447
1	1	2	7.152 872	6.540 124
1	0	3	− 0.015 209	− 1.421 678
1	1	3	− 25.820 810	67.313 793
1	0	4	0.851 250	− 0.097 543
1	0	5	− 0.303 191	1.706 157
2	0	0	− 0.261 773	0.894 413
2	1	0	− 65.590 140	12.641 198
2	2	0	− 1443.695 438	561.993 531
2	0	1	− 0.551 988	0.994 855
2	1	1	67.665 722	− 29.843 219
2	0	2	0.157 490	1.580 799
2	1	2	181.952 908	144.223 878
2	0	3	− 2.478 166	− 2.531 431
2	0	4	− 1.986 866	− 3.578 547
3	0	0	− 1.068 208	− 0.139 399
3	1	0	− 89.134 210	− 180.674 123
3	0	1	− 7.747 853	11.880 138
3	1	1	− 43.679 204	− 352.908 770
3	0	2	1.140 281	− 6.552 610
3	0	3	28.356 612	42.887 331
4	0	0	4.689 580	− 5.934 924
4	1	0	438.770 088	2.294 425
4	0	1	− 2.780 916	14.829 801
4	0	2	21.503 060	− 45.486 291
5	0	0	37.969 141	30.593 030
5	0	1	40.015 850	272.205 108
6	0	0	133.329 614	292.803 732

(An error in an earlier program version was primarily responsible for the poorer agreement in Ref. 27.) Also computed are the matrix elements of the first through sixth powers of the expansion variables, evaluated in the basis set of one-dimensional functions. These matrix elements were used together with the full vibrational wave functions in the calculation of the dipole moment matrix elements.

The next step is to generate an expansion variable polynomial expression for the dipole moment function. As discussed elsewhere[11,12,29,30] it is necessary to transform from the valence angle bisector (VAB) reference frame used in the *ab initio* calculation to the Eckart frame; this transformation involves a rotation in the plane of the molecule by a small angle β. The case of symmetric triatomic molecules, such as the principal isotope of ozone, is discussed in further detail by Adler-Golden and Carney,[12] who present an analytical formula for β. This transformation was applied at each *ab initio* geometry, yielding the values of μ_x and μ_y, the Eckart frame analogs of the VAB dipole components defined in Sec. II. The resulting grids of μ_x and μ_y values were each least squares fitted to an expansion variable polynomial of the appropriate symmetry. The expansion coefficients obtained using MPMO variables are given in Table VI. The dipole function has been shifted to account for the difference between the CASSCF and experimental equilibrium geometries; as shown in Sec. VI, this gives improved agreement with the experimental permanent dipole moment. Since μ_x and μ_y are, respectively, even and odd upon interchange of r_1 and r_2, the μ_x function is in the same form as Eq. (5) and Appendix A potential functions, while for μ_y the plus sign in the numerator is changed to a minus sign. Finally, the dipole moment polynomial, the one-dimensional matrix elements, and the vibrational wave functions were combined to yield

the dipole moment matrix elements R. R is calculated somewhat differently for each combination of vibrational symmetries A and B:

$$R_{AB} = \langle A \,|\mu_y|\, B \rangle, \qquad (9a)$$

$$R_{AA} = \langle A \,|\mu_x|\, A \rangle, \qquad (9b)$$

$$R_{BB} = \langle B \,|\mu_x|\, B \rangle. \qquad (9c)$$

The $|A\rangle$ and $|B\rangle$ wave functions have, respectively, even and odd values of the asymmetric stretching quantum number v_3.

It should be noted that β and hence the orientations of

TABLE VII. Dipole moment matrix elements (ea_0) connecting the A and B vibrational states.

	(001)	(011)	(101)	(021)	(111)	(003)	(031)
(000)	− 0.068 12	0.003 30	− 0.015 34	0.000 43	0.001 66	0.003 85	− 0.000 24
(010)	− 0.006 55	− 0.067 52	− 0.002 58	− 0.005 40	− 0.014 92	0.001 80	− 0.001 08
(100)	− 0.011 21	− 0.002 39	0.065 50	− 0.000 46	− 0.002 62	− 0.007 86	0.000 91
(020)	0.000 24	0.009 86	− 0.000 15	− 0.066 82	0.003 92	− 0.000 72	− 0.007 47
(110)	− 0.004 24	− 0.011 45	0.006 77	0.003 46	0.064 95	− 0.001 77	0.001 04
(002)	0.093 28	0.009 48	− 0.018 43	0.000 00	− 0.007 17	− 0.108 02	0.003 39
(030)	− 0.001 30	− 0.000 67	0.000 65	0.012 82	0.000 48	− 0.001 34	− 0.066 03
(200)	0.023 10	0.000 62	0.012 49	− 0.000 03	0.002 52	0.001 71	− 0.000 39
(120)	− 0.000 11	0.007 01	− 0.000 23	− 0.012 00	− 0.010 42	0.000 06	0.004 37
(012)	− 0.004 73	0.092 65	− 0.003 82	− 0.014 07	− 0.018 50	− 0.011 40	0.000 65
(040)	0.000 11	− 0.001 55	0.000 24	0.001 19	0.001 25	− 0.000 50	− 0.015 72
(210)	0.000 49	0.021 40	0.004 97	− 0.000 74	0.013 06	0.000 25	0.000 19
(102)	− 0.020 59	− 0.003 36	− 0.087 66	− 0.000 15	− 0.010 38	− 0.026 78	0.002 05

	(201)	(121)	(013)	(041)	(211)	(103)
(000)	0.001 06	− 0.000 26	0.000 53	− 0.000 07	− 0.000 34	− 0.001 27
(010)	− 0.000 30	0.002 55	− 0.003 51	0.000 34	0.001 09	− 0.000 71
(100)	− 0.020 11	0.000 64	− 0.001 02	0.000 23	0.001 73	0.004 40
(020)	0.000 16	0.014 28	0.002 78	− 0.002 00	0.000 42	0.000 15
(110)	− 0.003 61	− 0.004 51	0.006 73	− 0.001 71	− 0.020 04	0.001 99
(002)	0.036 80	0.000 21	− 0.005 93	0.000 27	0.000 69	0.024 48
(030)	− 0.001 09	− 0.005 14	− 0.001 44	− 0.009 58	− 0.000 02	− 0.000 55
(200)	0.067 16	− 0.000 60	− 0.000 36	0.000 07	− 0.001 86	− 0.005 50
(120)	− 0.000 19	− 0.064 43	− 0.002 37	0.001 86	0.005 72	− 0.000 34
(012)	0.001 50	− 0.011 39	0.107 64	− 0.005 24	0.033 93	0.003 94
(040)	− 0.000 10	0.000 99	0.002 44	0.065 11	− 0.001 65	− 0.000 18
(210)	0.006 81	0.003 68	− 0.001 17	0.000 56	0.066 05	− 0.002 33
(102)	− 0.017 54	− 0.000 54	0.006 09	− 0.000 81	− 0.009 09	− 0.099 97

the Eckart frame x and y axes are dependent on the relative atomic masses. Therefore, slightly different dipole moment components would be obtained with different partially substituted isotopes. All calculations reported here pertain to the principal ozone isotope (mass of each O = 15.9997 amu). Another caveat is that our matrix element signs are specific to the phases of our numerical wave functions, a fact which must be considered when comparing the current results to calculations which employ a different phase convention.

V. RESULTS

Results for the dipole moment matrix elements connecting the first 13 vibrational states of each symmetry are presented in Tables VII through IX. For these calculations the $\alpha = 2.7192$ Å^{-1} MPMO potential energy surface was used with 224 basis functions of each symmetry. The dipole moment function was the sixth degree polynomial fit given in Table VI. The matrix elements are well converged with

TABLE VIII. Dipole moment matrix elements (ea_0) connecting the A vibrational states.

	(000)	(010)	(100)	(020)	(110)	(002)	(030)
(000)	− 0.213 76						
(010)	0.023 49	− 0.210 23					
(100)	0.006 57	0.000 18	− 0.208 99				
(020)	0.000 86	− 0.033 23	− 0.001 03	− 0.206 63			
(110)	− 0.002 81	0.005 48	0.022 56	− 0.000 55	− 0.205 49		
(002)	0.004 31	0.000 88	0.000 75	− 0.000 90	0.000 55	− 0.213 48	
(030)	0.000 05	− 0.001 75	0.000 03	− 0.040 66	0.001 82	0.000 18	− 0.202 86
(200)	0.002 33	0.000 15	0.010 52	0.000 92	0.000 34	− 0.002 01	0.000 18
(120)	− 0.000 03	0.003 93	0.000 85	0.004 27	− 0.031 82	0.000 54	− 0.001 09
(012)	− 0.000 71	0.004 11	0.000 95	− 0.001 35	0.001 60	0.022 77	0.001 18
(040)	0.000 04	0.000 20	− 0.000 22	0.002 90	0.000 03	0.000 24	0.046 85
(210)	0.000 04	0.002 28	− 0.004 01	− 0.000 24	0.009 16	− 0.000 15	− 0.002 04
(102)	− 0.000 83	− 0.000 26	0.003 49	0.000 03	0.000 67	0.004 94	− 0.000 08

	(200)	(120)	(012)	(040)	(210)	(102)
(200)	− 0.204 92					
(120)	− 0.001 40	− 0.201 92				
(012)	0.000 93	− 0.000 78	− 0.209 43			
(040)	0.000 09	− 0.002 70	0.000 30	− 0.198 63		
(210)	0.021 71	− 0.000 69	− 0.001 71	0.000 32	− 0.201 25	
(102)	0.001 43	− 0.000 11	− 0.000 10	0.000 01	0.000 68	− 0.208 58

TABLE IX. Dipole moment matrix elements (ea_0) connecting the B vibrational states.

	(001)	(011)	(101)	(021)	(111)	(003)	(031)
(001)	− 0.214 81						
(011)	0.023 15	− 0.211 02					
(101)	− 0.005 73	− 0.000 03	− 0.210 30				
(021)	0.001 04	− 0.032 71	0.001 07	− 0.207 15			
(111)	0.003 16	− 0.004 50	0.022 08	0.000 35	− 0.206 51		
(003)	0.005 66	0.001 20	− 0.000 41	− 0.002 27	− 0.000 69	− 0.210 57	
(031)	− 0.000 07	− 0.002 13	− 0.000 04	− 0.039 91	− 0.001 86	0.000 37	− 0.203 11
(201)	− 0.004 24	− 0.000 44	0.009 83	− 0.001 11	0.000 32	0.002 32	− 0.000 23
(121)	− 0.000 13	0.004 45	− 0.001 11	0.003 12	0.031 08	0.000 98	− 0.000 89
(013)	0.001 09	− 0.005 36	0.001 74	0.001 74	0.001 92	− 0.022 36	− 0.003 19
(041)	− 0.000 10	− 0.000 05	− 0.000 38	− 0.003 49	− 0.000 08	− 0.000 48	− 0.045 82
(211)	0.000 08	− 0.004 02	− 0.004 20	0.000 70	0.008 45	0.000 38	0.002 31
(103)	0.001 10	− 0.000 32	− 0.004 19	0.000 08	− 0.001 05	0.004 33	− 0.000 24

	(201)	(121)	(013)	(041)	(211)	(103)
(201)	− 0.207 14					
(121)	0.001 29	− 0.202 62				
(013)	0.001 61	0.000 93	− 0.206 29			
(041)	− 0.000 07	0.002 72	0.000 67	− 0.198 63		
(211)	0.021 30	0.000 61	− 0.001 97	0.000 36	− 0.203 00	
(103)	− 0.001 96	− 0.000 29	0.000 21	− 0.000 01	− 0.000 77	− 0.205 27

respect to the choice of potential energy surface, degree of the dipole moment polynomial, and number of basis functions. With a smaller basis set (147 functions), only a few of the matrix elements involving the higher-lying states change appreciably. In particular, the changes are small enough that the allowed $10 \mu \ v_3$ transitions are not appreciably affected. The use of SPF rather than MPMO expansion variables had an even smaller effect, as did the use of a fifth rather than a sixth degree dipole moment fit.

We conclude that the dipole moment matrix elements in Tables VII through IX do not significantly reflect either approximations in the vibrational wave functions or the manner in which the dipole moment function is fit, except possibly where forbidden transitions between high energy levels are involved. Thus, by comparing calculated infrared intensities [using Eq. (2)] with experimental values a direct test of the quality of the *ab initio* dipole moment is afforded.

VI. COMPARISON WITH EXPERIMENTAL VIBRATIONAL INTENSITIES

A. Survey of experimental data

A large amount of infrared absorption data exists for ozone, including many high resolution spectra which have been analyzed in detail. References 31 and 32 by Rothman *et al.* describe the AFGL atmospheric line parameter compilation, and provide a comprehensive survey of ozone spectra. To derive pure vibrational intensities from this data, care must be taken to account for the influence of Coriolis coupling, which mixes the rotational manifolds of adjacent bands. Where available, we have used deperturbed dipole moment matrix elements derived from rotation-vibration analyses. Another complication is the presence of hot bands arising primarily from the (0 1 0) state population, about 3% at room temperature. Table X lists the values which we have selected as the experimental pure vibrational band strengths. Rationales for choosing these values are presented below.

1. v_1 and v_3

We used the combined v_1 and v_3 band strength of 379.5 atm^{-1} cm^{-2} from Secroun et al.[33] and the dipole moment ratio R_3/R_1 of 9.4 $\pm$ 1 from Flaud et al.[34] The hot bands are included in the total band strength, and we assume that they contribute the same as the cold bands relative to their population. Therefore, no further correction is required to obtain the pure vibrational band strengths. We chose error bars of 5% for v_3 and 25% for v_1, which are probably generous in view of the excellent measurement precision reported in Ref. 33.

2. $v_1 + v_3$, $2v_3$, and $2v_1$

Flaud et al.[35] report dipole moment matrix element absolute values of 0.0383, 0.0082, and 0.0019 D for these respective bands based on a rotation-vibration intensity analysis. The band strengths are therefore given by Eq. (2) after converting from Debye to ea_0. Error bars were not reported,

TABLE X. Experimental and calculated pure vibrational band strengths (atm^{-1} cm^{-2} at 298 K).

Band	Experimental[a]	Calculated
v_2	17.4 $\pm$ 1.7	25.6
v_3	375 $\pm$ 19	320.0
v_1	4.5 $\pm$ 1.1	3.15
$2v_2$	$\cdots$[b]	0.07
$v_2 + v_3$	1.47 $\pm$ 0.15	1.24
$v_1 + v_2$	0.59 $\pm$ 0.12	0.94
$2v_3$	1.42 $\pm$ 0.28	2.53
$v_1 + v_3$	31.7 $\pm$ 3.2	32.9
$2v_1$	0.08 $\pm$ 0.02	0.79
$v_1 + v_2 + v_3$	0.81 $\pm$ 0.08	0.51
$3v_3$	3.0 $\pm$ 0.3	2.99
$2v_1 + v_3$	0.33 $\pm$ 0.07	0.24

[a] See the text for derivation of these values.
[b] Not observed.

however. We have assumed uncertainties of 10%, 20%, and 30% for the respective band strengths.

3. $v_1 + v_2 + v_3$

We used the band strength reported by Barbe *et al.*[36] of 0.78 atm^{-1} cm^{-2} which excludes hot bands, and renormalized by dividing by the room temperature Boltzmann population of the ground state. We chose 10% error bars.

4. v_2

We used the band strength [including the (0 1 0) hot band] of 18 atm^{-1} cm^{-2} from the low resolution study by McCaa and Shaw[37] and corrected for the factor of 2 greater intensity of the hot band as suggested by Goldman *et al.*[38] We chose 10% error bars.

5. $v_1 + v_2$, $v_2 + v_3$, $3v_3$, and $2v_1 + v_3$

We used the band strengths from McCaa and Shaw,[37] which are not corrected for Coriolis effects. For reasons discussed above in the case of the v_1 and v_3 bands, no further adjustment to account for hot bands is required. We chose 10% error bars for $v_2 + v_3$ and $3v_3$ and 20% error bars for the other two bands since they are much weaker and hence more susceptible to Coriolis effects.

6. $2v_2$

The observation of this band by McCaa and Shaw[37] has not been duplicated in subsequent studies, and has been ascribed to an impurity.[16] Thus, we conclude that the $2v_2$ band strength is less than the typical instrumental sensitivity in these studies, which is on the order of 0.1 atm^{-1} cm^{-2}.

7. Permanent dipole moment

The permanent dipole moment has been measured accurately by microwave spectroscopy, and has the absolute value 0.5324 ± 0.0024 D (0.210 ± 0.001ea_0).[15]

B. Comparison of experiment and theory

The calculated band strengths, derived from the dipole matrix elements in Tables VII through IX, are compared with the experimental values in Table X. The agreement is remarkably good for an *ab initio* calculation, especially considering that the values span three orders of magnitude. The only severe disagreement occurs for the $2v_1$ band, which according to Ref. 35 derives virtually all of its intensity in the room temperature spectrum via Coriolis coupling with the $v_1 + v_3$ band. It is particularly significant that even the weak transitions are well described since they are sensitive to the detailed shape of the dipole moment function and serve as a measure of the extent of deviation from harmonic oscillator selection rules. The deviation from harmonic behavior is not large, as evidenced by both the small size of the matrix elements for forbidden transitions and the fact that the harmonic scaling rule $R^2 \sim v$ is obeyed reasonably well for most of the $\Delta v = -1$ transitions. This is consistent with the small size of the high-order terms in the normal coordinate polynomial expansion (Appendix B).

The permanent dipole moment is given by the diagonal matrix elements in Tables VIII and IX. For the ground vibrational state the calculated value is -0.543 D, in excellent agreement with the experimental absolute value of 0.5324 ± 0.0024 D. This calculated value differs from (and is superior to) the value given in Table II mainly because as mentioned in Sec. IV the dipole function has been shifted to account for the difference between the *ab initio* and experimental equilibrium geometries. A slight dependence of the permanent dipole on vibrational excitation is predicted.

We believe that the CASSCF dipole moment function is sufficiently reliable that most of the Table VII through IX matrix elements are of comparable accuracy to those of the corresponding cold bands in Table X, especially for the well-converged states listed in Table V. Moreover, for the strongly allowed 10 μ v_3 bands we expect an accuracy of several percent in the band strengths relative to the (0 0 1) fundamental. This very good relative accuracy is expected in view of the approximately harmonic behavior described above.

VII. DISCUSSION

The calculated dipole moment matrix elements will be very useful for the analysis of ozone 10 μ v_3 emission spectra which have been observed in the atmosphere and in the laboratory. According to recent observations in the COCHISE experiment[3] the most heavily populated levels in ozone formed from recombination are the states $(0\ 0\ N)$, $N = 1$ through 5, and $(1\ 0\ N)$, $N = 1$ through 4. In Table VII the relevant v_3 matrix elements are given for N of up to 3. It is found that the harmonic scaling mentioned above, used previously[2] to analyze the COCHISE data, is approximately obeyed for both $(0\ 0\ N)$ and $(1\ 0\ N)$ states. It also holds reasonably for levels containing additional excitation in the bending mode. Thus, more accurate relative values derived from Table VII matrix elements will not have a large impact on the analysis of v_3 hot band emission.

As for the radiative properties of ozone vibrational levels which are higher in energy than those studied here, it seems unlikely that any drastic change in this roughly harmonic behavior will occur until both the level density and mode coupling are sufficient to set up accidental resonances. A region of extensive resonances, which might appropriately be termed "quantum chaos,"[39] seems to occur in ozone at very high vibrational energies, judging from the appearance of dense line clusters in the resonance Raman spectrum.[40] In order for theory to reliably address questions about the properties of these very high-lying levels both a larger vibrational basis set and a more accurate potential energy function would be required.

Concerning atmospheric absorption spectra of ozone, the current calculation may suggest improved intensity values for a number of hot bands, particularly for forbidden transitions where harmonic or separable mode approximations may break down. Predicted intensities for the stronger hot bands are given in Table XI using the calculated dipole moment matrix elements. Accurate experimental values for these bands have not to our knowledge been published. In general, the predictions agree roughly with expectations. However, there is one surprising result: a heretofore unob-

TABLE XI. Calculated strengths of selected hot bands, Boltzmann factor not included.

Transition	$\tilde{v}/\mathrm{cm}^{-1}$ [a]	$S/\mathrm{atm}^{-1}\,\mathrm{cm}^{-2}$ at 298 K
$2v_2 - v_2$	698.4	51.0
$v_2 + v_3 - v_3$	684.4	24.3
$v_2 + v_1 - v_1$	692.2	23.3
$v_2 + v_1 - v_2$	1025.6	309.3
$2v_3 - v_3$	1015.9	584.7
$v_1 + v_3 - v_1$	1007.7	286.0
$v_1 + v_2 - v_2$	1094.4	2.2
$v_1 + v_3 - v_3$	1068.7	2.3
$2v_1 - v_1$	1098.2	8.0
$v_1 + v_2 + v_3 - v_2$	2084.3	30.7
$v_1 + 2v_3 - v_3$	2042.0	57.3
$2v_1 + v_3 - v_1$	2082.6	55.7
$2v_1 - v_3$	1159.2	40.9

[a] From Refs. 16 and 26.

served hot band, the forbidden transition (0 0 1)–(2 0 0) at 1159 cm^{-1}, is predicted to have a remarkably large band strength of about 40 atm^{-1} cm^{-2} (0.27 atm^{-1} cm^{-2} using a 298 K Boltzmann factor). Indeed, this band is strong enough to be included in the AFGL atmospheric absorption line atlas.[32] This surprisingly large intensity is caused by borrowing from the strong (0 0 1)–(0 0 2) transition via Darling–Dennison resonance.[16,41] Presumably the reason why the 1159 cm^{-1} band has not yet been observed is that it lies within the wings of the stronger v_1 and v_3 bands. However, it might show up in high resolution spectra. A detailed re-examination of high resolution spectra in this region would be very desirable.

An important benefit of the quantitative agreement which we have obtained between experimental and calculated band strengths is that the signs of the dipole moment matrix elements have now been established for these bands. With the sign ambiguities removed it should be possible to refine the ozone dipole moment function to give essentially perfect agreement with experimental dipole moment matrix elements; this in turn would yield even more accurate band strength predictions. Unfortunately, there are a number of different ways in which the dipole moment can be adjusted, and it is not clear to us which way is best. Not only are there many more expansion coefficients necessary for an accurate fit than there are available band strengths, there are also different expansions possible depending on the choice of variables. However, if additional experimental intensity data become available, or if appropriate theoretical constraints on the functional form of the dipole moment could be applied, refinement of the dipole moment function for ozone could be accomplished with greater confidence.

APPENDIX A: THE MPMO POTENTIAL ENERGY FUNCTION

The MPMO potential energy function is written

$$V = r_e^2 \sum_{ijk} C_{ijk}(y_1^i + y_2^i)(y_1 y_2)^j y_3^k / (1 + \delta_{0i}),$$

where the y_i are defined in Eqs. (6)–(8). The C_{ijk} are related to the Dunham coefficients K_{ijk} as follows:

$$C_{200} = K_{200}, \quad C_{010} = K_{010},$$

$$C_{101} = K_{101}, \quad C_{002} = K_{002},$$

$$C_{300} = K_{300} + \gamma K_{200},$$

$$C_{110} = K_{110} + \tfrac{1}{2}\gamma K_{010},$$

$$C_{201} = K_{201} + \tfrac{1}{2}\gamma K_{101},$$

$$C_{011} = K_{011}, \quad C_{102} = K_{102}, \quad C_{003} = K_{003},$$

$$C_{400} = K_{400} - \tfrac{7}{12}\gamma^2 C_{200} + \tfrac{3}{2}\gamma C_{300},$$

$$C_{210} = K_{210} + \gamma C_{110} - \tfrac{1}{6}\gamma^2 C_{010},$$

$$C_{020} = K_{020} - \tfrac{1}{4}\gamma^2 C_{010} + \gamma C_{110},$$

$$C_{301} = K_{301} - \tfrac{1}{6}\gamma^2 C_{101} + \gamma C_{201},$$

$$C_{111} = K_{111} + \tfrac{1}{2}\gamma C_{011},$$

$$C_{202} = K_{202} + \tfrac{1}{2}\gamma C_{102},$$

$$C_{012} = K_{012}, \quad C_{103} = K_{103}, \quad C_{004} = K_{004},$$

where $\gamma = \alpha r_e$.

APPENDIX B: NORMAL COORDINATE REPRESENTATION OF THE OZONE CASSCF DIPOLE MOMENT FUNCTION

For the benefit of workers who employ normal coordinate methods we have fit the CASSCF dipole moment components to polynomials in the dimensionless normal coordinates q_i pertaining to O^{16} ozone. The polynomials are

$$\mu_{x,y} = \sum_{ijk} \mu_{ijk}\, q_1^i\, q_2^j\, q_3^k, \tag{B1}$$

where $i + j + k \leqslant 6$; k is even for μ_x and odd for μ_y. In our sign convention positive q_3 corresponds to positive Δr_1 and negative Δr_2. The fit was performed by first transforming each ab initio geometry to symmetry coordinates S_i (using the equations in Ref. 12) and then linearly transforming to the q_i using the quadratic force constants of Ref. 16; next, the dipole moment components μ_x and μ_y were least squares fit to the function (B1). The following coefficients μ_{ijk} were obtained:

μ_x/ea_0				μ_y/ea_0			
i	j	k	μ_{ijk}	i	j	k	μ_{ijk}
0	0	0	− 0.207 730	0	0	1	− 0.095 921
0	0	2	− 0.005 741	0	0	3	− 0.001 492
0	0	4	0.000 294	0	0	5	0.000 024
0	0	6	− 0.000 003				
0	1	0	0.032 824	0	1	1	− 0.000 263
0	1	2	0.000 124	0	1	3	− 0.000 168
0	1	4	− 0.000 034	0	1	5	0.000 002
0	2	0	0.000 392	0	2	1	0.000 695
0	2	2	0.000 053	0	2	3	0.000 030
0	2	4	0.000 001				
0	3	0	− 0.000 152	0	3	1	− 0.000 038
0	3	2	− 0.000 004	0	3	3	0.000 001
0	4	0	0.000 004	0	4	1	0.000 004
0	4	2	− 0.000 001				
0	5	0	− 0.000 001	0	5	1	− 0.000 001
0	6	0	0.000 000				
1	0	0	0.009 154	1	0	1	0.018 339
1	0	2	0.000 046	1	0	3	0.000 429
1	0	4	− 0.000 015	1	0	5	− 0.000 005
1	1	0	− 0.004 120	1	1	1	− 0.001 264
1	1	2	− 0.000 114	1	1	3	0.000 083
1	1	4	0.000 007				
1	2	0	0.000 035	1	2	1	− 0.000 012
1	2	2	0.000 031	1	2	3	− 0.000 012
1	3	0	− 0.000 006	1	3	1	− 0.000 003
1	3	2	0.000 000				
1	4	0	0.000 009	1	4	1	0.000 000
1	5	0	− 0.000 001				
2	0	0	0.002 701	2	0	1	− 0.000 534
2	0	2	0.000 005	2	0	3	− 0.000 051
2	0	4	− 0.000 001				
2	1	0	0.000 048	2	1	1	0.000 098
2	1	2	0.000 053	2	1	3	− 0.000 008
2	2	0	− 0.000 085	2	2	1	− 0.000 021
2	2	2	− 0.000 012				
2	3	0	− 0.000 012	2	3	1	0.000 003
2	4	0	0.000 003				
3	0	0	− 0.000 065	3	0	1	− 0.000 132
3	0	2	0.000 036	3	0	3	0.000 004
3	1	0	− 0.000 029	3	1	1	− 0.000 008
3	1	2	− 0.000 007				
3	2	0	0.000 003	3	2	1	0.000 005
3	3	0	0.000 002				
4	0	0	− 0.000 064	4	0	1	0.000 008
4	0	2	− 0.000 003				
4	1	0	− 0.000 010	4	1	1	0.000 002
4	2	0	0.000 005				
5	0	0	− 0.000 002	5	0	1	0.000 000
5	1	0	0.000 002				
6	0	0	0.000 001				

As mentioned in Sec. IV, the partitioning of μ into these specific x and y components pertains only to the fully substituted ozone isotopes as a consequence of the mass dependence of the x and y axes in the Eckart frame.

[1]T. C. Degges, A. T. Stair, Jr., R. M. Nadile, and E. R. Hegblom, EOS Trans. AGU **60**, 338 (1979).

[2]W. T. Rawlins, G. E. Caledonia, and J. P. Kennealy, J. Geophys. Res. **86**, 5247 (1981).

[3]W. T. Rawlins, H. C. Murphy, G. E. Caledonia, J. P. Kennealy, F. X. Robert, A. Corman, and R. A. Armstrong, Appl. Opt. **23**, 3316 (1984).

[4]S. Huzinaga, J. Chem. Phys. **42**, 1293 (1965).

[5]T. H. Dunning, Jr., J. Chem. Phys. **53**, 2823 (1970).

[6]F. B. van Duijneveldt, IBM Research Report RJ 945, 1971.

[7]P. J. Hay and T. H. Dunning, Jr., J. Chem. Phys. **67**, 2290 (1977).

[8]B. O. Roos, Int. J. Quantum Chem. Quantum Chem. Symp. **14**, 175 (1980).

[9]P. E. M. Siegbahn, J. Amlof, A. Heiberg, and B. O. Roos, J. Chem. Phys. **74**, 2384 (1981).

[10]P. J. Hay, T. H. Dunning, Jr., and W. A. Goddard III, J. Chem. Phys. **62**, 3912 (1975).

[11]G. D. Carney, S. Giorgianni, and K. N. Raio, J. Mol. Spectrosc. **80**, 158 (1980).

[12]S. M. Adler-Golden and G. D. Carney, Chem. Phys. Lett. **113**, 582 (1985).

[13]L. A. Curtiss, S. R. Langhoff, and G. D. Carney, J. Chem. Phys. **71**, 5016 (1979).

[14]T. Tanaka and Y. Morino, J. Mol. Spectrosc. **33**, 538 (1970).

[15]M. Lichtenstein, J. J. Gallagher, and S. A. Clough, J. Mol. Spectrosc. **40**, 10 (1971).

[16]A. Barbe, C. Secroun, and P. Jouve, J. Mol. Spectrosc. **49**, 171 (1974).

[17]P. Hennig and G. Strey, Z. Naturforsch. Teil A **31**, 244 (1976).

[18]C. W. Wilson, Jr. and D. G. Hopper, J. Chem. Phys. **74**, 595 (1981).

[19]K. S. Sorbie and J. N. Murrell, Mol. Phys. **29**, 1387 (1975).

[20]J. N. Murrell, K. S. Sorbie, and A. J. C. Varandas, Mol. Phys. **32**, 1359 (1976).

[21]S. Carter, I. M. Mills, J. N. Murrell, and A. J. C. Varandas, Mol. Phys. **11**, 1 (1982).

[22]G. Simons, J. Chem. Phys. **61**, 369 (1974).

[23]G. D. Carney, L. A. Curtiss, and S. R. Langhoff, J. Mol. Spectrosc. **61**, 371 (1976).

[24]I. I. Tugov and V. P. Chernyavsky, J. Mol. Spectrosc. **99**, 302 (1983).

[25]J. N. Huffaker, J. Chem. Phys. **64**, 3175 (1976).

[26]V. M. Devi, S. P. Reddy, K. N. Rao, J. M. Flaud, and C. Camy-Peyret, J. Mol. Spectrosc. **77**, 156 (1979).

[27]D. Cropek and G. D. Carney, J. Chem. Phys. **80**, 4280 (1984).

[28]G. D. Carney, Thesis, Allegheny College, PA, 1983; D. Cropek, Thesis, Allegheny College, PA 1983.

[29]G. D. Carney, L. L. Sprandel, and C. W. Kern, Adv. Chem. Phys. **37**, 305 (1978).

[30]W. C. Ermler and B. J. Krohn, J. Chem. Phys. **67**, 1360 (1977).

[31]L. S. Rothman, Appl. Opt. **20**, 791 (1981).

[32]L. S. Rothman, R. R. Gamache, A. Barbe, A. Goldman, J. R. Gillis, L. R. Brown, R. A. Toth, J. -M. Flaud, and C. Camy-Peyret, Appl. Opt. **22**, 2247 (1983).

[33]C. Secroun, A. Barbe, P. Jouve, P. Arcas, and E. Arie, J. Mol. Spectrosc. **85**, 8 (1981).

[34]J. -M. Flaud, C. Camy-Peyret, and L. S. Rothman, Appl. Opt. **19**, 655 (1980).

[35]J. -M. Flaud, C. Camy-Peyret, A. Barbe, C. Secroun, and P. Jouve, J. Mol. Spectrosc. **80**, 185 (1980).

[36]A. Barbe, C. Secroun, A. Goldman, and J. R. Gillis, J. Mol. Spectrosc. **100**, 377 (1983).

[37]D. J. McCaa and J. H. Shaw, J. Mol. Spectrosc. **25**, 374 (1968).

[38]A. Goldman, J. R. Gillis, D. G. Murcray, A. Barbe, and C. Secroun, J. Mol. Spectrosc. **96**, 279 (1982).

[39]D. W. Noid, M. L. Koszykowski, and R. A. Marcus, Annu. Rev. Phys. Chem. **32**, 267 (1981).

[40]D. G. Imre, J. L. Kinsey, R. W. Field, and D. H. Katayama, J. Phys. Chem. **86**, 2564 (1982).

[41]B. T. Darling and D. M. Dennison, Phys. Rev. **57**, 128 (1940).